Magnetic Resonance in Medicine 51:518–524 (2004)

Cortical Depth-Dependent Gradient-Echo and Spin-Echo BOLD fMRI at 9.4T

Fuqiang Zhao,[1,2] Ping Wang,[1,2] and Seong-Gi Kim*[1,2]

To examine cortical depth-related spatial specificity and signal changes in gradient-echo (GE) and spin-echo (SE) blood oxygenation level-dependent (BOLD) fMRI signals, a well-established cat visual stimulation model was used at 9.4T. The GE BOLD signal percent change is the highest at the surface of the cortex containing pial vessels, and decreases as cortical depth increases. In contrast, the SE BOLD signal is more specific to parenchyma, showing the highest signal change in the middle cortical areas. The stimulation-induced ΔR_2^* to ΔR_2 ratio is dependent on the vessel size, which is related to basal susceptibility effects. The averaged ratio of ΔR_2^* to ΔR_2 in all active regions, including large vessels, is 3.3 ± 0.5 (N = 6). The averaged ratio of ΔR_2^* to ΔR_2 is 8.8 ± 1.7 (N = 4) on the surface of the cortex with large pial draining vessels, and decreases to 1.9 ± 0.1 on the middle cortical areas with parenchymal microvessels. $\Delta R_2^*/\Delta R_2$ is closely related to basal susceptibility effects and can be used to differentiate tissue from vessel regions. Magn Reson Med 51:518–524, 2004. © 2004 Wiley-Liss, Inc.

Key words: brain mapping; functional MRI; neural activity; cortical layer; high fields

Although blood oxygenation level-dependent (BOLD) contrast is widely used (1), its vascular signal source is not completely understood (for review see Ref. 2). The BOLD signal induced by deoxyhemoglobin arises from extravascular (EV) and intravascular (IV) components of small (i.e., radius $< \sim 8$ μm) and large venous blood vessels. The EV contribution from large vessels is linearly dependent on magnetic fields (B_0), whereas the microvascular EV effect increases supralinearly with B_0 (2–5). Thus, high magnetic fields increase the relative contribution of the microvascular EV component of BOLD signals. Furthermore, at high magnetic fields, T_2 of pure blood water (e.g., 5–7 ms at 9.4T) is much shorter than tissue T_2 (e.g., 40 ms at 9.4T), resulting in a significant reduction of the IV BOLD component when the echo time (TE) matches tissue T_2 or T_2^* (6). Therefore, the BOLD signal at higher fields is more specific to tissue. This has been confirmed experimentally (7,8). The highest *statistical* change in standard gradient-echo (GE) BOLD fMRI is observed in the parenchyma during somatosensory stimulation in rats at high fields of 7–11.7T (6,9–11), which indicates that the GE BOLD technique at high magnetic fields is adequate for tissue-specific functional imaging. However, the highest GE BOLD *percent* changes exist in the large draining veins at 9.4–11.7T, because the EV effect of large vessels still contributes to the GE BOLD signal (6,10,11). This component can be removed by the use of spin-echo (SE) BOLD fMRI because the dephasing effect, which is generated by the field inhomogeneity around large vessels, can be refocused by a 180° pulse (6,12). Thus, the spatial specificity of GE BOLD fMRI should be further examined by comparison with SE BOLD fMRI, which will provide insight into the source of high-resolution BOLD signals.

The GE BOLD signal is dependent on inhomogeneous magnetic fields induced by deoxyhemoglobin, while the SE BOLD signal is dependent only on irreversible diffusion-related averaging in inhomogeneous fields. Diffusion-related signal averaging is more sensitive to smaller vessels at higher magnetic fields (3–5,13). Thus, when the size of detectable vessels decreases, the ratio of stimulation-induced R_2^* (= $1/T_2^*$) to R_2 (= $1/T_2$) changes ($\Delta R_2^*/\Delta R_2$) is expected to decrease up to 1.0. At higher magnetic fields, $\Delta R_2^*/\Delta R_2$ decreases as the signal contribution from the smaller vessels increases (3–5). Therefore, it is important to compare ΔR_2 and ΔR_2^* for different vessel sizes and magnetic field strengths to understand BOLD signal sources. At 1.5T, the average $\Delta R_2^*/\Delta R_2$ is 3.3–4.0 in various human cerebral cortical areas (14–16). At 3T, the average $\Delta R_2^*/\Delta R_2$ in the human motor cortex is 3.6 (17). At 9.4T, the average $\Delta R_2^*/\Delta R_2$ is 3.3 in the rat somatosensory cortex (12). These data do not support the notion that $\Delta R_2^*/\Delta R_2$ decreases at higher magnetic fields. Since the diffusion-related effect at higher fields increases predominantly in the tissue and less in the large vessel regions, it is necessary to compare region-specific ΔR_2^* and ΔR_2.

In this study, cortical depth-related GE BOLD and SE BOLD fMRI signals were compared at 9.4T using a well-established cat visual stimulation model (18–21). During visual stimulation, GE BOLD signal changes at 4.7T were observed both in gray matter of the visual cortex and at the surface of the cortex with pial vessels (18,19); therefore, this model can be used to examine the specificity of BOLD signals. Furthermore, this visual stimulation induces the highest neural activity at layer IV in the primary visual cortex due to direct thalamocortical projection. Thus, we can examine whether the middle cortical layers have the highest BOLD signal. For separation of cortical depth-related regions with similar vascular environments, a local susceptibility effect induced by vessels can be utilized (13). An iron oxide contrast agent was administered at the end of most the studies to enhance the static susceptibility effect, which is useful for image segmentation of cortical regions.

[1]Department of Neurobiology, University of Pittsburgh, Pittsburgh, Pennsylvania.

[2]Center for Magnetic Resonance Research, University of Minnesota, Minneapolis, Minnesota.

Grant sponsor: National Institutes of Health; Grant numbers: EB00337; EB00332; NS44589; EB00201; RR08079; Grant sponsors: Keck Foundation; McKnight Foundation Neuroscience Endowment.

*Correspondence to: Seong-Gi Kim, Brain Imaging Research Center, Department of Neurobiology, University of Pittsburgh, 3025 E. Carson St., Pittsburgh, PA 15203. E-mail: kimsg@pitt.edu

Received 13 March 2003; revised 13 October 2003; accepted 13 October 2003.

DOI 10.1002/mrm.10720
Published online in Wiley InterScience (www.interscience.wiley.com).

© 2004 Wiley-Liss, Inc.

MATERIALS AND METHODS

Animal Preparations and Stimulation

Six female adolescent cats (0.75–1.6 kg, 11–16 weeks old) were used with approval from the Institutional Animal Care and Use Committee at the University of Minnesota. Details of the experimental protocol were published previously (19,20). Briefly, the animals were mechanically ventilated under isoflurane anesthesia (1–1.3% v/v) in a 1:1 N_2O:O_2 mixture. The femoral artery and vein were catheterized for physiological monitoring and the administration of contrast agents, respectively. The animal was placed in a cradle and restrained in a normal postural position by a custom-designed head frame. End-tidal CO_2 level was kept within normal physiology ranges (3.0–3.8%), body temperature was controlled at 38.5°C, and mean blood pressure was maintained within 80–105 mmHg. The binocular visual stimuli consisted of high-contrast, *drifting* square-wave gratings (two cycles per second) of vertical orientation. *Stationary* gratings of identical spatial frequency were presented during the rest period.

MR Experiments

All NMR measurements were performed on a 9.4T/31-cm horizontal magnet (Magnex, UK) equipped with an actively shielded 11-cm-diameter gradient-insert (Magnex, UK), and interfaced to a Unity INOVA console (Varian). A surface coil of 1.6 cm diameter was positioned on top of the cat head. Multislice fast low-angle shot (FLASH) images were acquired to identify anatomical structures in the brain and to position a slice of interest in the isocenter of the magnetic field. Magnetic field homogeneity was optimized by manual volume-localized shimming or by a fast, automatic shimming technique by mapping along projections (FASTMAP) (22), yielding a water spectral line width of 13–28 Hz.

From multislice "scout" GE BOLD fMRI studies, a single 2-mm coronal plane perpendicular to the surface of the cortex was chosen. For anatomical reference, T_1-weighted images of the slice chosen for functional studies were obtained by the four-segment EPI technique with an inversion time of 1.4 s, a field of view (FOV) of 2×2 cm^2, and a matrix size of 128×128. GE EPI images with TEs of 6, 8, 10, 13, 16, 19, 23, 25, 29, 34, 40, and 50 ms were obtained to measure T_2^*. For BOLD fMRI studies, single-shot EPI images were obtained with a matrix size of 64×64 and an FOV of 2×2 cm^2. To reduce the effective TE, the zero *k*-space line was shifted by 24 *k*-space lines from the center of a data acquisition period. The GE BOLD fMRI parameters were: TE = 10, 15, 20, and 25 ms; repetition time (TR) for a single image = 0.5 s; and effective TR for four TE images = 2.0 s. An Ernst flip angle was chosen to maximize steady-state signals. A typical stimulation paradigm for GE BOLD fMRI included the acquisition of 30 control (60 s), 20 stimulation, and 30 control images. SE BOLD fMRI was performed with a double-echo EPI sequence (6,12), with TE = 30, 40, and 50 ms; TR for a single image = 2 s; and effective TR = 6 s for three TE images. Adiabatic half- and full-passage pulses were used for 90° and 180° pulses, respectively. The stimulation paradigm for SE BOLD fMRI included the acquisition of 10 control (60 s), 10 stimulation, and 10 control images. For all animals, 10–15 GE and SE data sets were obtained in an interleaved manner. The same number of trials was averaged for GE and SE BOLD fMRI. After fMRI studies, 10 mg Fe/kg dextran-coated monocrystalline iron oxide nanoparticles (MION) was injected into the femoral vein of four animals to enhance relative static susceptibility differences.

FMRI Data Analysis

Cross-correlation coefficient (CCC) maps were obtained using a boxcar cross-correlation method (23) with a typical CCC threshold of 0.3. A minimal cluster size for an active region of 3 pixels was further imposed, and the effective *P*-value was $< 1 \times 10^{-4}$ (24). Percent-change maps were then obtained from "active" pixels that passed a statistical threshold. For depth-specific GE and SE fMRI changes, rectangular sections within the cortex were selected, and pixels along lines perpendicular to the dorsal surface and the cortical layers were determined. To average signals at the same depth, pixels were spatially interpolated using the nearest-neighbor resampling method (25), and then averaged signal profiles across cortical layers were plotted as a function of distance from the surface of the cortex.

Sequential data sampling was used, and thus images with different TEs were acquired at different time points. When a dynamic signal change induced by stimulation occurs, a direct comparison between temporally unmatched TE data may yield erroneous results. To solve this problem, linear temporal interpolation was performed. The baseline period consisted of 36 s of prestimulation control data to ensure that magnetization had reached equilibrium, while the activation data were defined as the period of 6–30 s after the onset of stimulation.

To determine whether R_2 and R_2^* changes were region-specific, five susceptibility regions were chosen based on histograms in the studies with subsequent MION injection. One region of interest (ROI) was composed of all activated pixels from a previous GE BOLD fMRI experiment with TE of 20 ms, and contained both tissue and large vessels. This ROI was further subdivided, based on the basal susceptibility effect, which is directly related to vessel size and density (13). To determine relative susceptibility effects in active pixels, R_2^* changes induced by MION ($\Delta R_{2\text{MION}}^*$) were calculated on a pixel-by-pixel basis using T_2^*-weighted images with 12 TE values, and grouped into four $\Delta R_{2\text{MION}}^*$ regions with the same number of pixels. These same ROIs were used for further data analyses whether or not the pixels were "active." ROI-based R_2 and R_2^* during baseline were calculated by fitting logarithmic TE-dependent signal intensities to a linear function. To calculate ROI-based stimulation-induced ΔR_2 or ΔR_2^*, the percent changes of averaged signals within an ROI were plotted as a function of TE. Since the signal percent change can be approximated by $-\Delta R_2 \times$ TE or $-\Delta R_2^* \times$ TE, a slope of the linearly fitted line is $-\Delta R_2$ or $-\Delta R_2^*$. All values are reported as mean ± standard deviation (SD), and error bars on graphs are standard errors of mean (SEM).

RESULTS

Comparison of GE BOLD and SE BOLD fMRI Maps

Figure 1 shows statistical and percent-change maps of GE BOLD fMRI with TE of 20 ms, and SE BOLD fMRI with TE

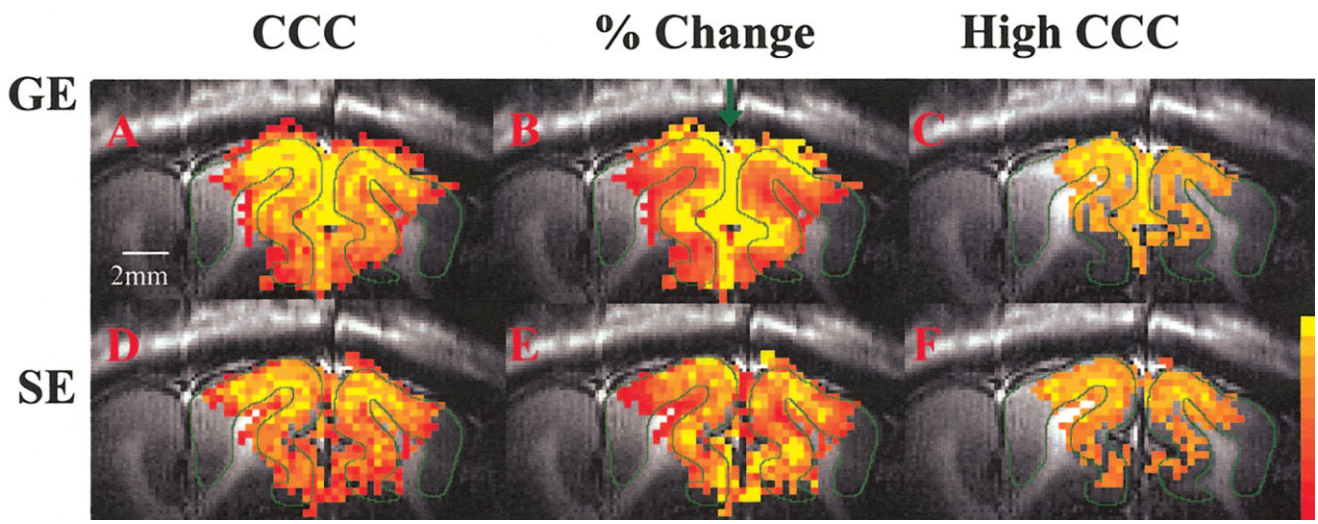

FIG. 1. Activation maps of (**a–c**) GE and (**d–f**) SE BOLD fMRI of one representative cat overlaid on T_1-weighted EPI images. From multiple-TE data, the results for only one TE value are shown here: 20 ms for GE fMRI, and 40 ms for SE fMRI. **a** and **d:** Statistical maps with a cross-correlation coefficient threshold of 0.3. **b** and **e:** Percent-change maps calculated for statistically significant pixels. **c** and **f:** Statistical maps with 238 active pixels, which is half the total number of active pixels shown in **a**. This corresponds to a CCC threshold of 0.69 in GE BOLD fMRI and 0.57 in SE BOLD fMRI. Green contours obtained from T_1-weighted EPI images indicate the lateral cortices in both hemispheres, where the visual cortex is located. The top of the images is dorsal. The color bar indicates a range of CCC values between 0.3 (red) and 0.9 (yellow) for **a–f**, percent changes between 0.2% and 4% for **b**, and percent changes between 0.2% and 2% for **e**. A green arrow indicates the vessel area between the two hemispheres.

of 40 ms. Statistical maps were obtained using the cross-correlation method with a threshold CC value of 0.3 (Fig. 1a and d). Percent changes were calculated only in statistically active pixels (Fig. 1b and e). Although the difference between contrast-to-noise ratios (CNRs; average signal change/average pixel-by-pixel SD) is not statistically significant, the highest CNR for GE BOLD fMRI with TE of 20 ms is 3.5, while the highest CNR for SE BOLD fMRI with TE of 40 ms is 2.2. Thus, 20-ms GE and 40-ms SE data were selected for comparison. To directly compare GE and SE results, the same number of pixels with the highest statistical values were then chosen (Fig. 1c and f). The number of active pixels shown in Fig. 1c and f is half the number of active pixels shown in Fig. 1a.

In the GE BOLD fMRI maps, many pixels with high statistical values (yellow color) are located within the gray matter area (green contours of Fig. 1a and c) and between the two hemispheres. The highest percent-signal change (yellow in Fig. 1b) occurred on the dorsal surface of the visual cortex and between the two hemispheres (indicated by an green arrow) where large draining veins are located. This is consistent with our previous observations at 4.7T (18,19,21). In SE BOLD fMRI of the same animal (Fig. 1d and f), the highest statistical value (yellow) is located at the middle of the cortex. Signal changes at the surface of the cortex and between the two hemispheres were significantly reduced, indicating improvements of spatial localization to the neural activity area. Generally, highly significant regions of statistical maps (Fig. 1d) colocalize with high percentage changes (Fig. 1e). In the TE data for all of the animals, similar GE and SE BOLD activation patterns were observed. It should be noted that stimulation-induced signal changes in Fig. 1 contain non-TE-dependent components, including inflow effects, which can be separated from ΔR_2 or ΔR_2^* using multiecho fMRI data (see Materials and Methods).

Figure 2 shows averaged profiles of GE and SE BOLD fMRI signals from six animals across cortical layers without using any statistical threshold. Signals of pixels at the same depth within ROIs were averaged. The surface of the cortex is at zero, and deeper cortical regions are represented by larger positive distances. Approximate boundaries of cortical layers, obtained from the literature (26), are also shown. The GE BOLD percent-signal change was the highest near the edge of the brain and was also significant outside the cortex (indicated by a negative distance). The GE BOLD change decreases when pixels are distant from the surface of the cortex. This observation is consistent with previous GE BOLD measurements at 9.4T (6,10) and 11.7T (11). In contrast to the GE BOLD signal, the SE BOLD signal is maximal at a cortical depth of around 0.7–1.2 mm, which is located at layer IV. The high SE BOLD signal change was also observed at cortical layers V and VI. In the white-matter area (~2.0 mm deep), significant signal changes were still observed, possibly due to a partial-volume contribution from adjacent gray matter.

Quantitative Comparison Between R_2 and R_2^* Changes

In the absence of stimuli, contrast agents can highlight regional differences in the static susceptibility effect. Figure 3 shows the effect of administering the exogenous contrast agent MION. All pixels that were activated in the earlier GE BOLD fMRI study (Fig. 1a) were selected for calculation of $\Delta R^*_{2\mathrm{MION}}$ values in Fig. 3a. In the histogram of $\Delta R^*_{2\mathrm{MION}}$ (Fig. 3b), vertical bars indicate the boundaries of the four magnetic susceptibility regions, which were chosen such that each contained the same number of pix-

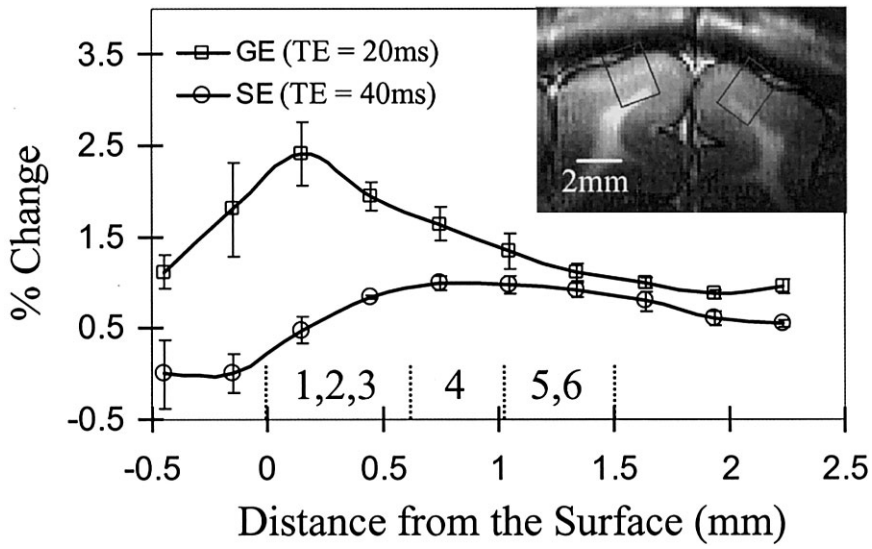

FIG. 2. GE and SE BOLD fMRI percent signal changes as a function of cortical depth in the cat visual cortex. Inset shows a T_1-weighted image with two rectangular sections, chosen for the depth-specific signal analysis. Data from GE (TE = 20 ms) and SE (TE = 40 ms) BOLD fMRI were used without a statistical threshold. The dorsal surface of the cortex is at zero, and increasingly positive distances indicate deeper cortical regions. Approximate schematic boundaries between the upper (layers 1–3), middle (layer 4), and lower (layers 5 and 6) cortical layers are also shown as dashed vertical bars, based on data from the literature (26). Spatial resolution of the data points is 300 μm. GE BOLD percent changes monotonically decrease with depth, but SE BOLD percent changes are minimal at the surface of the cortex. Error bars are SEM (N = 6 animals).

els. $\Delta R^*_{2\mathrm{MION}}$ maps (Fig. 3c–f) show that the static susceptibility effect is highest at the surface of the cortex (Fig. 3f), and decreases with cortical depth. The high susceptibility effect on the surface of the cortex is likely due to the contribution of large surface vessels with 65–190 μm radius (27). The average $\Delta R^*_{2\mathrm{MION}}$ values for four animals in these four ROIs were 50 ± 0.3 s^{-1} (Fig. 3c), 58 ± 4 s^{-1} (Fig. 3d), 67 ± 9 s^{-1} (Fig. 3e), and 89 ± 18 s^{-1} (Fig. 3f). These four susceptibility regions were used for further quantitative analyses.

Figure 4 shows basal R_2 and R^*_2 values (Fig. 4a) and stimulation-induced R_2 and R^*_2 changes (Fig. 4b) in the four previously-segmented susceptibility regions. An average SD error in the fitting of each R_2 and R^*_2 calculation was 3.5% and 2.1%, respectively. Average errors in the fitting of depth-specific ΔR_2 and ΔR^*_2 were 12.4% and 9.3%, respectively. The basal R_2 value in the entire active region (22.0 ± 1.3 s^{-1} (N = 6)) is consistent with our previous 9.4T measurement of 25.6 s^{-1} for rat somatosensory cortex (6). Baseline T^*_2 values obtained using GE data with 12 TE values (6–50 ms) were 34 ± 4 ms (N = 6) in gray matter, and 25 ± 3 ms in white matter, which agrees well with the value of 31 ms for the entire active region obtained from baseline fMRI data with four TEs (10–25 ms). Our T^*_2 value of cat visual cortex at 9.4T is slightly longer than that of human brain at 7T, 25 ms (8). Since T^*_2 is dependent on basal physiological conditions and vascular structure, as well as shimming, it is difficult to compare across species and regions. From baseline R_2 and R^*_2 (Fig. 4a), an apparent transverse relaxation rate induced by local susceptibility effect (R_2') can be calculated as defined by $R^*_2 - R_2$. Depth-dependent R'_2 is correlated with $\Delta R^*_{2\mathrm{MION}}$ (R_2 = 0.97, N = 4 regions, data not shown).

In the entire active region, stimulation-induced ΔR^*_2 and ΔR_2 were −0.62 ± 0.22, and −0.19 ± 0.06 s^{-1} (N = 6), respectively. Similar to findings shown in Fig. 2, ΔR^*_2 is the highest at the surface of the cortex, and decreases as cortical depth increases (Fig. 4b). Unlike ΔR^*_2, ΔR_2 is the lowest at the surface of the cortex. Stimulation-induced $\Delta R'_2$ change ($\Delta R^*_2 - \Delta R_2$) is linearly correlated with basal R'_2 (R_2 = 0.997) (Fig. 4c). The average $\Delta R^*_2/\Delta R_2$ ratio in the entire active region is 3.3 ± 0.5 (N = 6). The highest R'_2 is from the cortical surface, where the stimulation-induced $\Delta R^*_2/\Delta R_2$ of 8.8 ± 1.7 (N = 4) is also the highest (Fig. 4c). At the middle and lower cortical regions with parenchymal microvessels, $\Delta R^*_2/\Delta R_2$ is the lowest, with a value of 1.9 ± 0.1 (N = 4). Our data demonstrate that $\Delta R^*_2/\Delta R_2$ is closely dependent on the basal R'_2 effect, which is related to anatomical and vascular structures.

DISCUSSION

Spatial Specificity of GE BOLD and SE BOLD fMRI at 9.4T

GE BOLD contrast has been used in high-resolution fMRI studies because it is easy to implement and yields a high CNR (19,28–30). However, our data show that GE BOLD contrast contains significant large-vessel contributions at 9.4T. Since the cortical surface containing large draining vessels can be easily detected by standard imaging approaches, we can apply a filter to remove activation pixels outside the cortical area. However, the upper cortical region (i.e., supragranular layers) has higher signal changes than the middle cortical region (i.e., granular layer IV). It is not clear what portion of the GE BOLD signal change at the upper cortical region originates from actual tissue or surface vessels. Thus, there is an intrinsic problem in obtaining high-spatial-resolution fMRI with the GE BOLD technique. When large regions are active during stimulation, as in the current study, the GE BOLD technique is not suit-

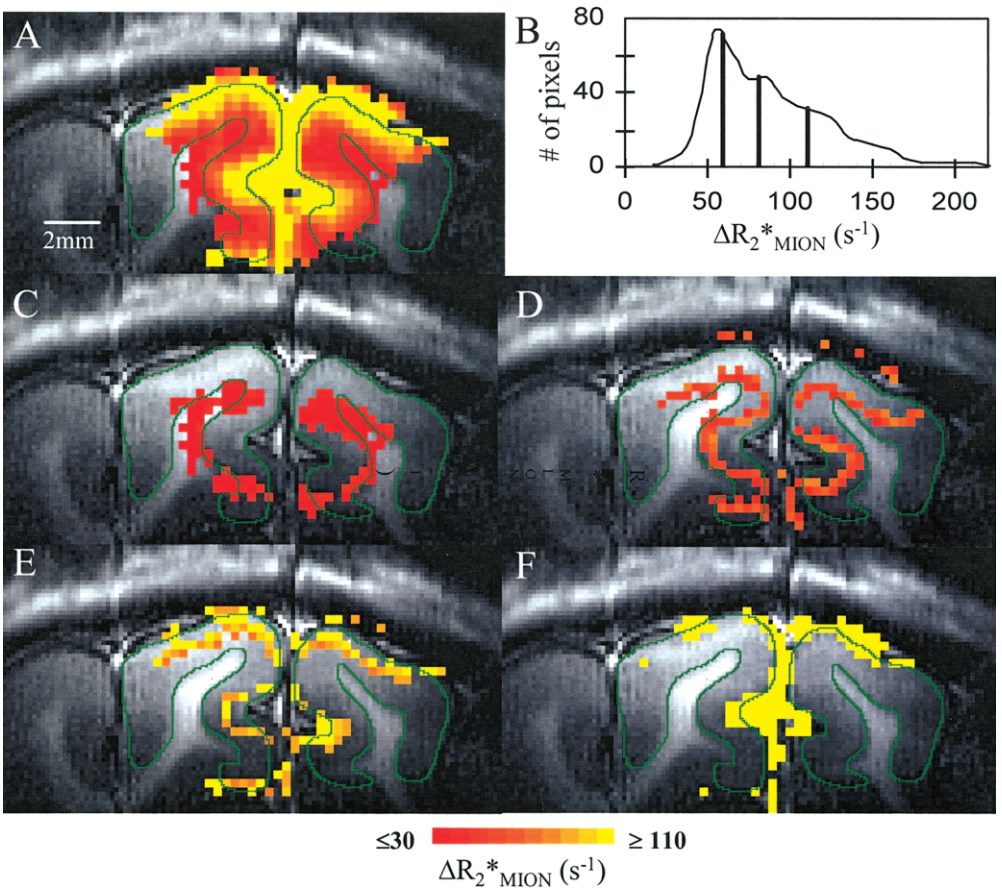

FIG. 3. Susceptibility regions determined by contrast agent-induced R_2^* changes (ΔR_{2MION}^*). **a:** ΔR_{2MION}^* values were calculated for all pixels that had shown statistically significant activation in the earlier GE BOLD (TE = 20 ms) fMRI study. **b:** Based on the histogram of ΔR_{2MION}^*, four susceptibility regions with the same number of pixels were segmented using the threshold of the ΔR_{2MION}^* indicated by vertical bars. **c–f:** ΔR_{2MION}^* maps of these regions. Clearly, ΔR_{2MION}^* and cortical depth are correlated. These four regions were used to calculate the cortical depth-specific R_2 and R_2^* changes shown in Fig. 4. Color bar indicates ΔR_{2MION}^* in units of s^{-1}.

able for submillimeter high-resolution brain mapping. However, if the activation area is small and the draining problem is very minimal, the GE BOLD technique is a viable method for high-resolution fMRI, as shown in a previous study (9) in which a single barrel field was localized.

The high specificity results from a significant reduction of EV and IV contributions of draining vessels to the SE BOLD signal (6). With a typical venous blood volume of $<4\%$ in parenchymal areas (31), the IV contribution to the SE BOLD signal at 9.4T is estimated to be $<0.1\%$ (32). However, at ultra-high-resolution fMRI, a venous volume fraction can be 10–20% of a pixel, or even higher at the cortical surface. In this case, the relative SE BOLD signal change can be 0.3–0.6% at a TE of 40 ms when venous oxygenation levels increase from 0.7 (commonly observed in animal studies) to 0.8 (6,32). This suggests that an IV contribution to SE BOLD fMRI can be significant, depending on the venous blood volume fraction.

Dependency of $\Delta R_2^*/\Delta R_2$ on Static Susceptibility Effect and Magnetic Field

At a given blood volume, stimulation-induced EV ΔR_2^* increases as vessel size increases up to a radius of 8–10 μm (Fig. 1 in Ref. 13) and then remains constant. However, EV ΔR_2 is maximal at vessels with a radius of ~3–5 μm, and decreases dramatically as vessel size increases. Thus, a voxel with vessels $>$ 3–5 μm radius (containing a larger susceptibility effect) will have a larger EV $\Delta R_2^*/\Delta R_2$ (see Fig. 6 in Ref. 3). In a previous study (3) employing a computer simulation with a susceptibility effect of 40 Hz, the stimulation-induced $\Delta R_2^*/\Delta R_2$ was >7.0 when the vessel radius was >20 μm, and decreased to 1.7 when the vessel radius was 2.5 μm. In the current study, the high $\Delta R_2^*/\Delta R_2$ at the surface of the cortex indicates that a large vessel contribution is dominant at the surface, while $\Delta R_2^*/\Delta R_2$ of 1.9 at the middle and lower cortical regions suggests that the contribution of parenchymal microvessels is predominant.

In order to compare $\Delta R_2^*/\Delta R_2$ with results from different magnetic fields, we used a large ROI containing both tissue and draining vessel contributions for comparison with previously published ROI studies. In this study, the $\Delta R_2^*/\Delta R_2$ at 9.4T was 3.3 in cat visual cortex, which is consistent with a previously-described $\Delta R_2^*/\Delta R_2$ of 3.3 in rat somatosensory cortex at 9.4T (12). These 9.4T values are similar (albeit a little lower) to those from low magnetic fields. At 1.5T, the average stimulation-induced $\Delta R_2^*/\Delta R_2$

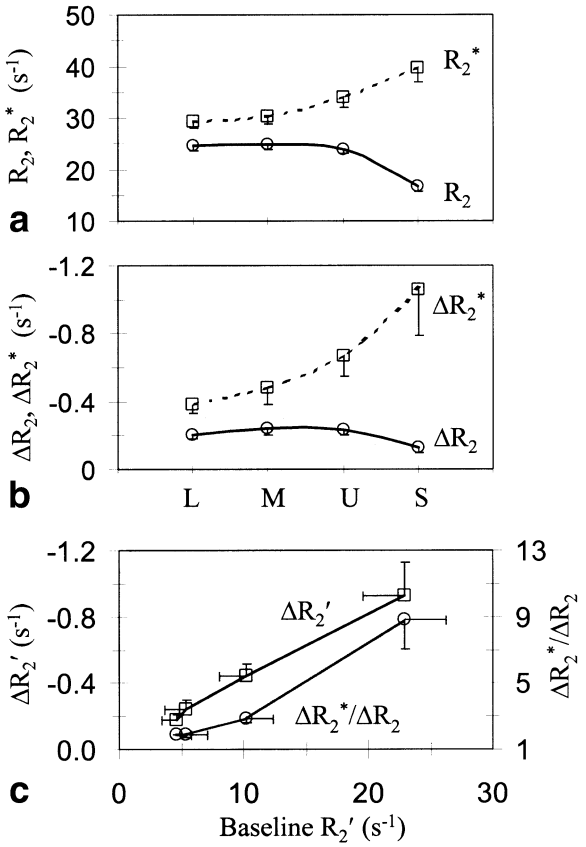

FIG. 4. Cortical depth-specific relaxation rate changes ($N = 4$). Baseline R_2 and R_2^* (**a**) and their stimulation-induced changes (ΔR_2 and ΔR_2^*) (**b**) were calculated within ROIs. L, lower cortical region; M, middle cortical region; U, upper cortical region; S, surface of cortex. Baseline R_2' was obtained by subtracting R_2 from R_2^*, and $\Delta R_2'$ was calculated by subtracting ΔR_2 from ΔR_2^*. **c:** Stimulation-induced $\Delta R_2'$ and $\Delta R_2^*/\Delta R_2$ are plotted as a function of baseline R_2'. The order of points with increasing R_2' (i.e., from left to right) is also L, M, U, and S in **c**. Stimulation-induced susceptibility change is linearly correlated with the basal susceptibility effect. $\Delta R_2^*/\Delta R_2$ is dependent on the static susceptibility effect, resulting in a dependence on cortical depth. For clarity, only one side of the error bar is shown.

was 3.5 in human motor cortex (14) and 3.3–4.2 in human visual cortex (15). At 3T, the average $\Delta R_2^*/\Delta R_2$ in human motor cortex was 3.6 (17). A dependence of $\Delta R_2^*/\Delta R_2$ on magnetic field strength up to 9.4T was not observed, which appears to contradict the predictions based on BOLD modeling (3–5,13).

In MR modeling, only the EV contribution has been considered (3–5,13). However, experimental data indicate that the IV and EV components contribute to BOLD signals; thus, it is possible that a field-dependent IV contribution may explain this discrepancy. During increased neural activation, the T_2 of blood itself will change when the deoxyhemoglobin content is altered, leading to signal changes in SE BOLD images. Assuming that the spin density of tissue and blood water is the same, the T_2-weighted MRI signal intensity S can be described by

$$S/S_0 = (1 - \nu)e^{-\mathrm{TE}/\mathrm{T}_{2(\mathrm{tissue})}} + \nu e^{-\mathrm{TE}/\mathrm{T}_{2(\mathrm{blood})}},$$

where S_0 is the signal intensity at TE of 0 ms, ν is the venous blood volume fraction, and $T_{2(\mathrm{tissue})}$ and $T_{2(\mathrm{blood})}$ are the transverse relaxation times of tissue and venous blood, respectively.

Assuming a venous oxygenation level increase from 0.6 to 0.7, T_2 of blood changes from 127 ms to 163 ms at 1.5T (33), and from 4.9 ms to 6.4 ms at 9.4T (6). Typically, spin TE is set to the T_2 value of tissue: 90 ms at 1.5T (34), and 40 ms at 9.4T (6). Assuming there are no changes in tissue T_2 and ν during neural stimulation, the relative signal change induced by blood T_2 change can be calculated using the above equation (e.g., 0.895% at 1.5T and 0.002% at 9.4T when ν is 0.04). The effective R_2 change induced by the IV contribution to the entire ROI ($\Delta R_{2(\mathrm{IV})}$) can be estimated using a relative signal change $= -\mathrm{TE} \times \Delta R_2$. When ν is 0.04, $\Delta R_{2(\mathrm{IV})}$ is -0.099 s^{-1} at 1.5T and -0.005 s^{-1} at 9.4T. It should be noted that effective $\Delta R_{2(\mathrm{IV})}$ differs from the actual R_2 change in pure blood. Our simplified approach assumes that the experimentally measured ΔR_2 is a sum of $\Delta R_{2(\mathrm{IV})}$ and $\Delta R_{2(\mathrm{EV})}$, where $\Delta R_{2(\mathrm{EV})}$ is the effective EV ΔR_2. Similarly, ΔR_2^* is the sum of $\Delta R_{2(\mathrm{IV})}^*$ and $\Delta R_{2(\mathrm{EV})}^*$, where $\Delta R_{2(\mathrm{IV})}^*$ and $\Delta R_{2(\mathrm{EV})}^*$ are the effective IV and EV ΔR_2^*, respectively. Since dynamic averaging is dominant in blood, $\Delta R_{2(\mathrm{IV})}^*$ is similar to $\Delta R_{2(\mathrm{IV})}$. At 1.5T, experimental ΔR_2^* and ΔR_2 were -0.55 and -0.16 s^{-1}, respectively (14). After subtracting the IV contribution of -0.099 s^{-1}, $\Delta R_{2(\mathrm{EV})}^*$ and $\Delta R_{2(\mathrm{EV})}$ at 1.5T are -0.451 s^{-1} and -0.061 s^{-1}, respectively, at ν of 4%; thus, the ratio of $\Delta R_{2(\mathrm{EV})}^*$ to $\Delta R_{2(\mathrm{EV})}$ at 1.5T is 7.4. Although we may have underestimated the estimated IV contribution to BOLD signals at 1.5T (35,36), this exercise demonstrates the importance of the IV contribution to $\Delta R_2^*/\Delta R_2$. At 9.4T, experimental ΔR_2^* and ΔR_2 in our studies were -0.63 and -0.19 s^{-1}, respectively. EV $\Delta R_{2(\mathrm{EV})}^*/\Delta R_{2(\mathrm{EV})}$ at 9.4T is 3.3 at ν of 4%. Our calculation suggests that a ratio of $\Delta R_{2(\mathrm{EV})}^*$ to $\Delta R_{2(\mathrm{EV})}$ decreases dramatically when magnetic fields increase, which agrees with theoretical predictions (3,5,13). Further systematic studies are needed to examine the field dependence of EV $\Delta R_2^*/\Delta R_2$.

CONCLUSIONS

The GE BOLD signal at 9.4T is contaminated by large vascular contributions. In fact, the largest signal change occurs at the large draining veins, including the surface vessels. Thus, the GE BOLD signal is not tissue-specific and is not suitable for high-resolution submillimeter imaging. In contrast to GE BOLD fMRI, SE BOLD fMRI at 9.4T improves the signal specificity to tissue. Stimulation-induced $\Delta R_2^*/\Delta R_2$ is closely related to cortical depth. Regions with high $\Delta R_2^*/\Delta R_2$ are located at the surface of the cortex with large draining vessels, while $\Delta R_2^*/\Delta R_2$ is low in tissue areas with parenchymal microvessels. Thus, $\Delta R_2^*/\Delta R_2$ can be used to separate tissue from large-vessel regions.

ACKNOWLEDGMENT

We thank Kristy Hendrich for her helpful comments and careful reading of this manuscript.

REFERENCES

1. Ogawa S, Lee T-M, Kay AR, Tank DW. Brain magnetic resonance imaging with contrast dependent on blood oxygenation. Proc Natl Acad Sci USA 1990;87:9868–9872.
2. Ogawa S, Menon RS, Kim S-G, Ugurbil K. On the characteristics of functional magnetic resonance imaging of the brain. Annu Rev Biophys Biomol Struct 1998;27:447–474.
3. Ogawa S, Menon RS, Tank DW, Kim S-G, Merkle H, Ellermann JM, Ugurbil K. Functional brain mapping by blood oxygenation level-dependent contrast magnetic resonance imaging. Biophys J 1993;64:800–812.
4. Weisskoff RM, Zuo CS, Boxerman JL, Rosen BR. Microscopic susceptibility variation and transverse relaxation: theory and experiment. Magn Reson Med 1994;31:601–610.
5. Kennan RP, Zhong J, Gore JC. Intravascular susceptibility contrast mechanisms in tissues. Magn Reson Med 1994;31:9–21.
6. Lee S-P, Silva AC, Ugurbil K, Kim S-G. Diffusion-weighted spin-echo fMRI at 9.4 T: microvasculuar/tissue contribution to BOLD signal change. Magn Reson Med 1999;42:919–928.
7. Gati JS, Menon RS, Ugurbil K, Rutt BK. Experimental determination of the BOLD field strength dependence in vessels and tissue. Magn Reson Med 1997;38:296–302.
8. Yacoub E, Shmuel A, Pfeuffer J, Van De Moortele P, Adriany G, Andersen P, Vaughan J, Merkle H, Ugurbil K, Hu X. Imaging brain function in humans at 7 Tesla. Magn Reson Med 2001;45:588–594.
9. Yang X, Hyder F, Shulman RG. Activation of single whisker barrel in rat brain localized by functional magnetic resonance imaging. Proc Natl Acad Sci USA 1996;93:475–478.
10. Duong TQ, Silva AC, Lee S-P, Kim S-G. Functional MRI of calcium-dependent synaptic activity: cross correlation with CBF and BOLD measurements. Magn Reson Med 2000;43:383–392.
11. Silva AC, Koretsky AP. Laminar specificity of fMRI onset times during somatosensory stimulation in rat. Proc Natl Acad Sci USA 2002;99:15182–15187.
12. Lee S-P, Silva AC, Kim S-G. Comparison of diffusion-weighted high-resolution CBF and spin-echo BOLD fMRI at 9.4 T. Magn Reson Med 2002;47:736–741.
13. Boxerman JL, Hamberg LM, Rosen BR, Weisskoff RM. MR contrast due to intravascular magnetic perturbations. Magn Reson Med 1995;34:555–566.
14. Bandettini PA, Wong EC, Jesmanowicz A, Hinks RS, Hyde JS. Spin-echo and gradient-echo EPI of human brain activation using BOLD contrast: a comparative study at 1.5 T. NMR Biomed 1994;7:12–20.
15. Jones D, Schirmer T, Lipinski B, Elbel G, Auer D. Signal undershoots following visual stimulation: a comparison of gradient and spin-echo BOLD sequences. Magn Reson Med 1998;40:112–118.
16. Lowe M, Lurito J, Mattews V, Phillips M, Hutchins G. Quantitative comparison of functional contrast from BOLD-weighted spin-echo and gradient-echo echoplanar imaging at 1.5 Tesla and H215O PET in the whole brain. J Cereb Blood Flow Metab 2000;20:1331–1340.
17. Jesmanowicz A, Bandettini PA, Wong EC, Tan G, Hyde JS. Spin-echo and gradient-echo EPI of human brain function at 3 Tesla. In: Proceedings of the 12th Annual Meeting of SMRM, New York, 1993. p 1390.
18. Duong TQ, Kim D-S, Ugurbil K, Kim S-G. Spatio-temporal dynamics of the BOLD fMRI signals: toward mapping submillimeter columnar structures using the early negative response. Magn Reson Med 2000;44:231–242.
19. Kim D-S, Duong TQ, Kim S-G. High-resolution mapping of iso-orientation columns by fMRI. Nat Neurosci 2000;3:164–169.
20. Duong TQ, Kim D-S, Ugurbil K, Kim S-G. Localized cerebral blood flow response at submillimeter columnar resolution. Proc Natl Acad Sci USA 2001;98:10904–10909.
21. Harel N, Lee S-P, Nagaoka T, Kim D-S, Kim S-G. Origin of negative blood oxygenation level-dependent fMRI signals. J Cereb Blood Flow Metab 2002;22:908–917.
22. Gruetter R. Automatic, localized in vivo adjustment of all first- and second-order shim coils. Magn Reson Med 1993;29:804–811.
23. Bandettini PA, Jesmanowicz A, Wong EC, Hyde JS. Processing strategies for time-course data sets in functional MRI of human brain. Magn Reson Med 1993;30:161–173.
24. Forman SD, Cohen JD, Fitzgerald M, Eddy WF, Mintun MA, Noll DC. Improved assessment of significant activation in functional magnetic resonance imaging (fMRI): use of a cluster-size threshold. Magn Reson Med 1995;33:636–647.
25. Grootoonk S, Hutton C, Ashburner J, Howseman AM, Joseph O, Rees G, Friston KJ, Turner R. Characterization and correction of interpolation effects in the realignment of fMRI time series. Neuroimaging 2000;11:49–57.
26. Payne BR, Peters A. The concept of cat primary visual cortex. In: Payne BR, Peters A, editors. The cat primary visual cortex. Academic Press; 2002. p 1–129.
27. Duvernoy H, Delon S, Vannson J. Cortical blood vessels of the human brain. Brain Res Bull 1981;7:519–579.
28. Frahm J, Merboldt KD, Henicke W. Functional MRI of human brain activation at high spatial resolution. Magn Reson Med 1993;29:139–144.
29. Menon RS, Goodyear BG. Submillimeter functional localization in human striate cortex using BOLD contrast at 4 Tesla: implications for the vascular point-spread function. Magn Reson Med 1999;41:230–235.
30. Cheng K, Waggoner R, Tanaka K. Human ocular dominance columns as revealed by high-field functional magnetic resonance imaging. Neuron 2001;32:359–374.
31. Grubb RL, Raichle ME, Eichling JO, Ter-Pogossian MM. The effects of changes in PaCO2 on cerebral blood volume, blood flow, and vascular mean transit time. Stroke 1974;5:630–639.
32. Duong TQ, Yacoub E, Adriany G, Hu X, Ugurbil K, Kim S-G. Microvascular BOLD contribution at 4 and 7T in the human brain: GE and spin-echo fMRI with suppression of blood effects. Magn Reson Med 2003;49:1019–1027.
33. Wright GA, Hu BS, Macovski A. Estimating oxygen saturation of blood in vivo with MR imaging at 1.5 T. J Magn Reson Imaging 1991;1:275–283.
34. Breger RK, Rimm AA, Fischer ME, Papke RA, Haughten VM. T_1 and T_2 measurements on a 1.5 Tesla commercial imager. Radiology 1989;171:273–276.
35. Boxerman JL, Bandettini PA, Kwong KK, Baker JR, Davis TL, Rosen BR, Weisskoff RM. The IV contribution to fMRI signal change: Monte Carlo modeling and diffusion-weighted studies in vivo. Magn Reson Med 1995;34:4–10.
36. Song AW, Wong EC, Tan SG, Hyde JS. Diffusion-weighted fMRI at 1.5T. Magn Reson Med 1996;35:155–158.